

An approach for projecting the timing of abrupt winter Arctic sea ice loss

Camille Hankel¹ and Eli Tziperman^{1,2}

¹Department of Earth and Planetary Sciences, Harvard University, 20 Oxford St, Cambridge, MA 02138

²School of Engineering and Applied Sciences, Harvard University

Correspondence: Camille Hankel (camille_hankel@g.harvard.edu)

1 **Abstract.** Abrupt and irreversible winter Arctic sea-ice loss may occur under anthropogenic warming due to the **collapse**
2 **disappearance** of a sea-ice equilibrium at a threshold value of CO₂, commonly referred to as a tipping point. Previous work
3 has been unable to conclusively identify whether a tipping point in **winter** Arctic sea ice exists because fully-coupled climate
4 models are too computationally expensive to run to equilibrium for many CO₂ values. Here, we explore the deviation of sea ice
5 from its equilibrium state under realistic rates of CO₂ increase to demonstrate **for the first time** how a few time-dependent CO₂
6 experiments can be used to predict the existence and timing of sea-ice tipping points without running the model to steady-state.
7 This study highlights the inefficacy of using a single experiment with slow-changing CO₂ to discover changes in the sea-ice
8 steady-state, and provides **an a novel** alternate method that can be developed for the identification of tipping points in realistic
9 climate models.

10 1 Introduction

11 The Arctic is warming at a rate at least twice as fast as the global mean with profound consequences for its sea ice cover.
12 **Summer sea ice** is already exhibiting rapid retreat with warming (Nghiem et al., 2007; Stroeve et al., 2008; Notz and Stroeve, 2016)
13 **especially in the summertime**, (Comiso and Parkinson, 2004; Nghiem et al., 2007; Stroeve et al., 2008; Notz and Stroeve, 2016; Stroeve
14 **shortening** the time that socioeconomic and ecological systems have to adapt. These concerns have motivated a large body
15 of work dedicated to both observing present-day sea ice loss (Kwok and Untersteiner, 2011; Stroeve et al., 2012; Lindsay
16 and Schweiger, 2015; Lavergne et al., 2019) and modeling sea ice to understand whether its projected loss is modulated by a
17 threshold-like or “tipping point” behavior. Abrupt loss **or a tipping point in of** Arctic sea ice could be driven by local positive
18 feedback mechanisms (Curry et al., 1995; Abbot and Tziperman, 2008; Abbot et al., 2009; Kay et al., 2012; Leibowicz et al., 2012; Burt et al.,
19 (Curry et al., 1995; Abbot and Tziperman, 2008; Abbot et al., 2009; Kay et al., 2012; Leibowicz et al., 2012; Burt et al., 2016; Feldl et al.,
20 **remote** feedback mechanisms that increase heat flux from the mid-latitudes (Holland et al., 2006; Park et al., 2015) (Holland et al., 2006; P
21 **or by** the natural threshold corresponding to the seawater freezing point (Bathiany et al., 2016). **Such a tipping point is**
22 **mathematically understood as** **If such an abrupt loss is caused by irreversible processes (typically, strong positive feedback mechanisms as c**
23 **it is referred to here as a “tipping point”**. A tipping point in the sense used here is a change in the number or stability of steady-
24 state solutions (Ghil and Childress, 1987; Strogatz, 1994) (Ghil and Childress, 1987; Strogatz, 1994) as a function of CO₂ and

25 is also known as a ~~“bifurcation”~~bifurcation. We note that some of the climate literature uses “tipping points” in a more general
26 sense of a relatively rapid change (e.g., Lenton, 2012). While most studies have concluded that there is no tipping point during
27 the transition from perennial to seasonal ice cover (i.e., during the loss of *summer* sea ice), the existence of a tipping point
28 during the loss of *winter* sea ice (transition to year-round ice-free conditions) continues to be debated in the literature (Eisen-
29 man, 2007; Eisenman and Wettlaufer, 2009; Notz, 2009; Eisenman, 2012), ~~with~~. Wagner and Eisenman (2015) showed that a
30 winter tipping point disappeared from a simple model of sea ice with no active atmosphere when a longitudinal dimension was
31 added. On the other hand, other literature (e.g., Abbot and Tziperman, 2008; Hankel and Tziperman, 2021) has demonstrated
32 the importance of atmospheric feedbacks, not included in the model of Wagner and Eisenman (2015), in inducing winter sea
33 ice tipping point. Furthermore, three out of seven ~~GCMs~~fully-complex Global Climate Models (GCMs) that lost their win-
34 ter sea ice completely in the CMIP5 Extended RCP8.5 Scenario ~~demonstrating an abrupt change that qualitatively looks like~~
35 showed a very abrupt change in winter Arctic sea ice resembling a tipping point ~~, and may be related to a bifurcation~~ (Hezel
36 et al., 2014; Hankel and Tziperman, 2021). However, given the projected rapid changes to CO₂ in the coming centuries and
37 the slower response of the climate system, we do not expect future sea ice to be fully equilibrated to the CO₂ forcing at a given
38 time, making the standard steady-state tipping point analysis challenging. Thus, ~~we are interested in projecting the timing of~~
39 our first goal is to understand abrupt winter Arctic sea ice ~~changes under changes—~~which may or may not be due to tipping
40 points—under rapidly changing CO₂ forcing, ~~when the standard steady-state tipping point analysis is not applicable~~where sea
41 ice is not at equilibrium.

42 Tipping points imply a bi-stability (meaning that sea ice can take on different values for the same CO₂ concentration),
43 and hysteresis — an irreversible loss of sea ice even if CO₂ is later reduced. ~~The computational efficiency of simple models~~
44 ~~allowed studies using them to calculate the region of winter sea ice bi-stability by running~~Bi-stability (and therefore tipping
45 points) can be tested for by running model simulations to steady-state at many different CO₂ values, which is ~~not possible~~
46 ~~with expensive~~computationally inefficient in expensive, state-of-the-art ~~Global Climate Models (GCMs)~~GCMs. GCM stud-
47 ies ~~therefore, therefore,~~ tend to use a single experiment with very gradual CO₂ increases and decreases (Li et al., 2013) or even
48 a faster CO₂ change (Ridley et al., 2012; Armour et al., 2011), ~~assuming~~and look for hysteresis in sea ice that would imply the
49 existence of a tipping point. These studies implicitly assume that such a run should approximate the behavior of the steady-state
50 at different CO₂ concentrations. However, Li et al. (2013) further integrated two apparently bi-stable points and found that they
51 equilibrated to the same value of winter sea ice: there was no “true” bi-stability at these two CO₂ concentrations, the sea ice
52 was simply out of equilibrium with the CO₂ forcing. This calls into question the current use of time-changing CO₂ runs to
53 study the bifurcation structure of sea ice.

54 In light of the difficulties in using climate model runs with time-changing CO₂ (hereafter “transient runs”) ~~for identifying~~
55 ~~tipping points, we identify a need,~~ the first goal of this work is to understand the relationship between these transient runs
56 and the steady-state value of sea ice ~~as a function of CO₂~~ in systems with and without bifurcations (since the existence of a
57 bifurcation in winter sea ice remains unknown), and the second goal is to develop a new efficient method for the identification
58 of tipping points from transient runs. Theoretical work in dynamical systems (Haberman, 1979; Mandel and Erneux, 1987;
59 Baer et al., 1989; Tredicce et al., 2004) and studies related to bi-stability in the Atlantic Meridional Overturning Circula-

60 tion (Kim et al., 2021; An et al., 2021) have examined systems with tipping points when the forcing parameter (CO₂ in our
61 case) changes in time at a finite rate, ~~and~~. They found that as the forcing parameter passes the bifurcation point, the system
62 continues to follow the old equilibrium solution for some time before it rapidly transitions to the new one. ~~This~~ Specifically,
63 (Kim et al., 2021; An et al., 2021) find that the width of the hysteresis loop of AMOC is altered by the rate of forcing changes—
64 this phenomenon is referred to as “rate-dependent hysteresis”. This rate-dependence occurs in their case in a system that also
65 has bi-stability and hysteresis in the equilibrium state. This type of analysis has, to our knowledge, not yet been applied in the
66 context of winter sea ice loss under time-changing CO₂ concentrations, nor compared in systems with and without a bifurcation
67 (that is, with and without an equilibrium hysteresis).

68 In order to analyze how the hysteresis ~~curve~~ of sea ice under time-changing forcing relates to the steady-state behavior of
69 sea ice, we run a simple physics-based model of sea ice (Eisenman, 2007), configured in three different scenarios: with a large
70 ~~region~~ CO₂ range of bi-stability, a small ~~region~~ range of bi-stability, and no bi-stability in the equilibrium. These three scenarios
71 span the range of possible behaviors of winter sea ice in state-of-the-art climate models. Each case is run with different rates
72 of CO₂ increase (ramping rates). We use results from this model and from an even simpler standard 1D dynamical system
73 to demonstrate that the convergence of the transient behavior (under time-changing forcing) to the equilibrium behavior is
74 very slow as a function of the ramping rate of CO₂. In other words, even climate model runs with very slow-changing CO₂
75 forcing may simulate sea ice that is considerably out of equilibrium near the period of abrupt sea ice loss. Finally, we propose
76 ~~an a novel~~ approach for uncovering the underlying equilibrium ~~behavior in behavior—and thus the existence and location of~~
77 tipping points—in comprehensive models where it is computationally ~~inefficient infeasible~~ to simulate steady-state conditions
78 for many CO₂ values. Such a method is important given the model-dependent nature of winter sea ice tipping points discussed
79 above; uncovering the existence of sea ice tipping points in GCMs, which are the most realistic representation of Arctic-wide
80 sea ice behavior that we have, is the next step toward understanding whether such tipping points exist in the real climate system.
81 Our goal has some parallels to that of Gregory et al. (2004), who used un-equilibrated GCM runs to deduce the equilibrium
82 climate sensitivity when fully-equilibrated runs were computationally infeasible.

83 ~~Some GCMs seem to exhibit a tipping point~~ As mentioned above, some GCMs exhibit an abrupt change in winter sea ice
84 that may be a tipping point, and others ~~don’t do not~~ (Hezel et al., 2014; Hankel and Tziperman, 2021). The reasons ~~are~~
85 ~~likely complex and likely~~ involve numerous differences in parameters and parameterizations. It is not obvious how to modify
86 parameters in a single GCM to display all of these different behaviors. Therefore, we choose to use an idealized model of sea
87 ice where we can directly produce different bifurcation behaviors to address our second goal and answer the question: is it
88 possible to identify the CO₂ at which tipping points occur without running the model to a steady state for many CO₂ values?
89 Answering such a question in a simple model is an obvious prerequisite to tackling the problem of identifying climate bi-
90 stability in noisy, high-dimensional, GCMs. In order to perform this analysis for each of the three scenarios mentioned above,
91 we modify the strength of the albedo feedback via the choice of surface albedo parameters. The albedo values used here to
92 generate the three scenarios are not meant to reflect realistic albedo values, but rather allow us to represent in a single model
93 the range of sea ice equilibria behaviors that may exist in different GCMs. We, therefore, follow in the footsteps of previous
94 studies (e.g., Eisenman, 2007) that have also changed parameters (~~the latent heat of fusion~~) outside of their physically relevant

95 regime in order to understand *summer* sea ice bifurcation behavior; here we follow the same approach to understand when a
96 *winter* sea ice bifurcation can be detected without running an expensive climate model to steady-state.

97 2 Methods

98 2.1 Sea ice model

99 The ~~Eisenman model~~ sea ice model used follows Eisenman (2007) almost exactly and its key features are depicted schematically
100 in Figure 1. The model contains four state variables: sea ice effective thickness (V , which is volume divided by the area of the
101 model grid box), sea ice area (A), sea ice surface temperature (T_i), and mixed layer temperature (T_{ml}) for a single box rep-
102 resenting the entire Arctic. ~~The~~ Subsequent versions of this sea ice model have been used in Eisenman and Wettlaufer (2009)
103 , Eisenman (2012), and Wagner and Eisenman (2015). Those versions are derived from the model used here, making a few
104 further modest simplifications (using a hyperbolic tangent function for surface albedo, assuming the ice surface temperature is
105 in a steady state, combining all prognostic variables into one, enthalpy) that do not affect the qualitative behavior of the model
106 (i.e., the nature of summer and winter sea ice bifurcations). We choose to implement the earlier model because it explicitly
107 represents the key physical variables of ice volume, area, ocean temperature, and ice temperature as prognostic variables —
108 as opposed to combining them all into a single enthalpy — and thus provides more transparency and interpretability. We,
109 therefore, do not expect our results to change if we use any of the later model versions.

110 In the model, the atmosphere is assumed to be in radiative equilibrium with the surface, and the model is forced with a
111 seasonal cycle of insolation, of poleward ~~heat transport~~ atmospheric heat transport from the mid-latitudes, and of local optical
112 thickness of the atmosphere, which represents cloudiness. ~~The~~ Sea ice growth and loss are primarily determined by the heat
113 budget at the bottom of the ice and are therefore set by the balance between ocean-ice heat exchanges, and heat loss through
114 the ice to the atmosphere. When conditions for surface melting are met (when the ice surface temperature is zero and net fluxes
115 on the ice are positive), all surface heating goes into melting ice and the surface albedo of the ice is set to the melt pond albedo.
116 The ocean temperature is affected by shortwave and longwave fluxes in the fraction of the box that is ice-free, and by ice-ocean
117 heat exchanges. When the ocean temperature reaches zero, all additional cooling goes into ice production while the ocean
118 temperature remains constant. The full equations of the sea ice model can be found in the original paper (Eisenman, 2007)
119 and in the online Supporting Information; here, we highlight a few minor ways in which our implementation differs. First,
120 for simplicity, we do not model leads, which in the original model were represented by capping the ice fraction at 0.95 rather
121 than 1. Second, we use an approximation to the seasonal cycle of insolation (Hartmann, 2015) using a latitude of 75N. The
122 atmospheric albedo is set to 0.425 to produce the same magnitude of the seasonal cycle as in the original model of Eisenman
123 (2007).

124 2.2 Setup of simulations

125 In our transient-forcing scenarios (described below), we vary CO_2 in time which affects the [prescribed near-surface atmospheric](#)
126 mid-latitude temperature ($T_{\text{mid-lat}}$) and the atmospheric optical depth (N), (see Supporting Information). Specifically, we
127 increase the annual mean of $T_{\text{mid-lat}}$ by 3°C per CO_2 doubling and N by a ΔN that corresponds to 3.7 W/m^2 per doubling.
128 All model parameters are as in [\(Eisenman, 2007\)](#) [Eisenman \(2007\)](#) except as mentioned below.

129 We configure the model in three different scenarios that yield a wide CO_2 range of bi-stability in winter sea ice (Scenario
130 1), a small range of bi-stability in winter sea ice (Scenario 2), and no bi-stability in winter sea ice (Scenario 3). We do so by
131 modifying the strength of the ice-albedo feedback by changing the albedos of bare ice (α_i), melt ponds (α_{mp}), and ocean (α_o),
132 as listed in Table S1.

133 In each of the three scenarios, we tune the model (by adjusting the mean and amplitude of the atmospheric optical depth) to
134 roughly match the observed seasonal cycle of ice thickness under pre-industrial CO_2 ($\sim 2.5\text{--}3.7\text{ m}$, Eisenman, 2007). We then
135 run each scenario with multiple CO_2 ramping rates (expressed in “years per doubling”) with an initial stabilization period (fixed
136 pre-industrial CO_2), a period of exponentially increasing CO_2 concentration (which corresponds to linearly increasing radiative
137 forcing), another period of stabilization at the maximum CO_2 , a period of decreasing CO_2 , and a final period of stabilization at
138 the minimum CO_2 value (see Supplemental Figure S2). Scenarios 2 and 3 are ramped to higher final CO_2 values than Scenario
139 1 so that they lose all their sea ice. We also directly calculate the steady-state behavior of the sea ice (as done in the original
140 study) by running many simulations with fixed CO_2 values until the seasonal cycle of all the variables stabilizes. Because we
141 expect multiple equilibria (which could be ice-free, seasonal ice, or perennial ice) at some CO_2 values in Scenarios 1 and 2, we
142 run these steady-state simulations starting with both a cold (ice-covered) and a warm (ice-free) initial condition in order to find
143 these different steady-states. In the ice-free initial condition runs, the ice-albedo feedback will still play an important role if the
144 temperature cools sufficiently for ice to develop. At CO_2 values for which the sea ice is [bistable](#)[bi-stable](#), the ice-free initial
145 condition evolves to a perennially ice-free steady-state, and the ice-covered initial condition evolves to a seasonally ice-covered
146 steady-state (seen by the dotted and dashed lines respectively in Figs. [1a and 1e](#)[2a and 2c](#)).

147 2.3 Cubic ODE

148 ~~It turns out the~~ [The](#) main points we are trying to make about the transient versus equilibrium behavior of winter sea ice near
149 a tipping point are not unique to the problem of winter sea ice, and in order to demonstrate this, we use the simplest math-
150 ematical model that can display tipping points, [following other studies that have also used such simple dynamical systems](#)
151 [\(Ditlevsen and Johnsen, 2010; Bathiany et al., 2018; Ritchie et al., 2021; Boers, 2021\)](#). The cubic ODE used, while much sim-
152 pler than the sea ice model above, has some of the key characteristics of the sea ice system (it is a non-autonomous system due
153 to the time-depending forcing and has saddle-node bifurcations), which allows for direct comparison between the two models.
154 The ODE equation,

$$155 \frac{dx}{dt} = -x^3 + \delta x + \beta(t), \quad \beta(t) = \beta_0 + \mu t, \quad (1)$$

156 contains a time-changing forcing parameter, $\beta(t)$ mimicking the effects of CO₂ in the sea ice model. We consider this differ-
157 ential equation in three scenarios, paralleling those used with the sea ice model: in Scenario 1, $\delta = 5$ leading to a wide region
158 of bi-stability; in Scenario 2, $\delta = 1$ leading to a narrow region of bi-stability, and finally, in Scenario 3, $\delta = 0$ leading to a
159 mono-stable system. The different values of δ , therefore, produce the same three scenarios that were achieved in the sea ice
160 model by modifying the strength of the ice-albedo feedback. We mimic the hysteresis experiments of the sea ice model with
161 a sequence of ramping up and ramping down (using different ramping rates, μ) with values of β ranging from -10 to 10 to
162 sweep the parameter space that contains the bifurcations. We calculate the steady-states with fixed values of β ($\mu = 0$), starting
163 with both a positive and a negative initial condition of x to yield two stable solutions when these exist.

164 We want to calculate the upper and lower CO₂ values of the hysteresis region in runs with time-changing (i.e., transient)
165 CO₂ forcing. We do so by calculating the CO₂ value at which the March sea ice area drops below a critical threshold (50% ice
166 coverage; results are insensitive to the specific value used) during increasing and decreasing CO₂ integrations: we denote these
167 CO₂ values CO_2^i and CO_2^d , respectively (see Supplemental Figure S9). The difference between CO_2^i and CO_2^d is referred to
168 below as the “~~transient~~ hysteresis width” of the rate-dependent hysteresis whether an equilibrium hysteresis exists or not; this
169 width approaches the width of bi-stability at very slow ramping rates.

170 **2.4 Predicting A new method for predicting the CO₂ of the sea ice tipping point**

171 One of our main goals (see Introduction) is to efficiently estimate the equilibrium behavior of sea ice, including the location of
172 tipping points, without running the model to a steady state for many CO₂ values. This would show that such estimation could
173 be calculated for GCMs where tipping points cannot be detected using steady-state runs due to their computational cost. In
174 order to estimate the values of CO_2^i and CO_2^d that would have occurred for an infinitely slow ramping rate (in other words, the
175 range of CO₂ for which there is bi-stability) ~~without having to run a model to equilibrium for all values of CO₂ forcing~~ using
176 only the transient runs, we fit a polynomial of the form $f(x) = mx^c + b$ to CO_2^i and CO_2^d as functions of the ramping rate
177 x . Because c is negative, the fitted parameter b represents the prediction of CO_2^i and CO_2^d at infinitely slow ramping rates,
178 i.e., in the steady state. We also calculate the uncertainty on the fitted parameter b by block-bootstrapping to account for auto-
179 correlation; see Supporting Information. Other fits to CO_2^i and CO_2^d as a function of ramping rates, such as an exponential
180 function $f(x) = a + b \exp(-cx)$ could in principle be used, although we found the fit to be less good in our case.

181 **3 Results**

182 In the following three subsections, we discuss the behavior of the sea ice model and the cubic ODE under time-changing
183 forcing, the relationship of the transient and equilibrium behaviors, and a method that we propose for inferring the exist-
184 ence and location of tipping points from the transient behavior. Equilibrium hysteresis refers here to the path-dependent
185 solution of a variable due to bi-stability and a bifurcation in the steady-state (in other words, the loop traced by the steady-state
186 solutions). The term “rate-dependent hysteresis” (An et al., 2021; Manoli et al., 2020) describes hysteresis loops that appear
187 in time-changing forcing runs (rather than in the steady state) and that depend on the rate of forcing change. In our analysis

188 "rate-dependent hysteresis" applies to both systems with and without equilibrium hysteresis: it refers to any differences in the
189 results for increasing vs. decreasing CO₂ simulations of sea ice that are altered by the rate of CO₂ change.

190 3.1 Transient response of Arctic winter sea ice to time-changing CO₂

191 Our goal in this section is to understand the relationship of winter sea ice forced with time-changing CO₂ to its equilibrium state,
192 both in cases with and without a sea ice tipping point. In Figs. Hb,d,f-2a,c,e, we plot the results of running all three scenarios
193 (wide range of bi-stability (Scenario 1), narrow range of bi-stability (2), and no bi-stability (3)) under time-changing (transient)
194 and fixed CO₂ values. In all scenarios, the experiments run with time-changing CO₂ exhibit transient-rate-dependent hysteresis;
195 the transient-hysteresis width (lower horizontal gray bar in Fig. 1a2a) is larger for faster ramping rates (Figs. 1a2a,c,e). For
196 Scenarios 1 and 2, which have a region of bi-stability and equilibrium hysteresis (upper gray bar in Fig. 2a), this corresponds to
197 a widening from the equilibrium hysteresis (that would exist even with infinitely slow ramping rates), while in Scenario 3, this
198 hysteresis occurs only in transient simulations and is due to the inertia in the system (the sea ice can't respond instantaneously
199 to forcing changes). In Scenarios 1 and 2, whose equilibrium solutions (dashed and dotted black lines in Fig. 12) have a tipping
200 point and therefore an infinite gradient of sea ice thickness vs. CO₂, the faster ramping rates also lead to more gradual (and
201 finite) gradient of sea ice thickness vs. CO₂. ~~The transient~~

202 The rate-dependent hysteresis loops across all scenarios at fast enough ramping rates (loops composed of the darkest blue
203 and darkest red) are qualitatively similar in shape, despite their different underlying steady-state structures. This similarity
204 indicates that from a single hysteresis run with time-changing CO₂ we cannot discern whether the underlying Arctic winter
205 sea ice equilibrium behavior has a region of bi-stability or not, nor how wide the region of true bi-stability is. In particular, a
206 single hysteresis loop found from a time-changing forcing simulation would always overestimate the width of bi-stability if
207 it was assumed to represent a quasi-steady state. This result demonstrates that the apparent transient-sea ice hysteresis loop
208 found by Li et al. Li et al. (2013) could be due to a system with or without a true hysteresis (i.e. bi-stability in the steady-state
209 behavior), consistent with their analysis without an equilibrium hysteresis, as they suggest, or due to a system with a narrower
210 equilibrium hysteresis than the one implied by their transient simulation.

211 ~~The robustness and generality of the above results of the sea ice model are now demonstrated by showing that the simpler~~
212 ODE (eqn. We now discuss the behavior of the simple cubic ODE (Eqn. 1) under similarly time-changing forcing. Previous
213 work in the dynamical systems literature (e.g., Haberman, 1979; Mandel and Erneux, 1987; Baer et al., 1989; Breban et al., 2003; Tredicce
214 has examined a variety of simple systems to understand the nature of bifurcations in the presence of a time-changing ("drifting"
215 or "transient") forcing parameter. In the climate literature as well (e.g., Ditlevsen and Johnsen, 2010; Bathiany et al., 2018; Ritchie et al., 20
216 , idealized dynamical systems similar to our Eqn. 1 have been used to understand the predictability of tipping points in the
217 presence of noise, and the ability to recover from such tipping points ("overshoot" scenarios). These works, as well as the
218 AMOC study of An et al. (2021), found that a system with a bifurcation that is run with a time-changing forcing parameter
219 can follow a given equilibrium value beyond the bifurcation value of the forcing parameter before undergoing the tipping point
220 transition to the new equilibrium value. This is consistent with the out-of-equilibrium behaviors we find for sea ice in Scenarios
221 1 and 2. To our knowledge, the simple ODE used here has not yet been analyzed with our specific goal in mind: to compare

222 the shape of rate-dependent hysteresis loops in generic dynamical systems both with and without bifurcations, and to address
223 the question of whether the equilibrium behavior can be inferred from the rate-dependent behavior of such systems.

224 ~~To address these two goals, we configure Eqn. 1) produces the same behavior. The 1D ODE is also configured analogously~~
225 to the sea ice model in three scenarios with wide bi-stability (Scenario 1), narrow bi-stability (Scenario 2), and no bi-stability
226 (Scenario 3) and force it with a time-changing forcing parameter. In Figs. ~~1b2b,d,f we see transient hysteresis in all scenarios,~~
227 we see that the three scenarios with similar dynamics (but different equilibrium structures) all display rate-dependent hysteresis,
228 similar to the result from the sea ice model. Specifically, even when there is only one stable equilibrium solution in both models
229 (Scenario 3, panels e and f), there is still a narrow region of ~~transient rate-dependent~~ hysteresis. Thus, we find that the ~~lack~~
230 ~~of distinction in transient hysteresis loops between systems with and without bifurcations and the widening of the hysteresis~~
231 ~~loop with increased forcing parameter ramping rate appear to be robust results across these dynamical systems. inability to tell~~
232 if rate-dependent hysteresis in Arctic winter sea ice is accompanied by an underlying equilibrium hysteresis appears to be a
233 generic feature of dynamical systems, which helps explain the challenges of interpreting the results of Li et al. (2013).

234 Mathematically, this 1D system is fundamentally different from the sea ice model because it is not periodically forced. We
235 show in the ~~supplementary Supporting Information~~ that adding a sinusoidal forcing term to the ODE does not qualitatively
236 change our results.

237 3.2 Slow convergence of the ~~transient rate-dependent~~ hysteresis to the equilibrium behavior

238 Our next objective is to demonstrate that it would require expensive runs in a GCM to approach the equilibrium behavior of sea
239 ice using slower and slower-changing CO₂ runs (hysteresis experiments). As we saw in Fig. ~~1, the 2,~~ the rate of loss of sea ice
240 with increasing CO₂ is ~~very abrupt in the equilibrium infinite~~ (dashed and dotted black lines) ~~and is infinite at the tipping point~~
241 in Scenarios 1 and ~~2, 2~~ at the tipping points. On the other hand, the gradient ~~is of sea ice thickness with respect to CO₂ is more~~
242 gradual and finite under time-changing forcing (blue and red curves) ~~but steepens as the ramping rate of CO₂ decreases.~~ We
243 now quantify the rate of this steepening by examining the maximum gradient of sea ice loss during each transient simulation
244 as a function of ramping rate (inverse of the years per doubling of CO₂). ~~Our objective is to demonstrate that it is difficult to~~
245 ~~approach the equilibrium behavior using slower and slower-changing CO₂ runs (transient hysteresis experiments).~~

246 In Fig. ~~2a3a,~~ we plot the maximum gradient of March sea ice thickness *with respect to CO₂* during each hysteresis experi-
247 ment, as a function of the CO₂ ramping rate. In Scenarios 1 and 2 (wide and narrow bi-stability, respectively), the maximum
248 gradient gets greater as the ramping rate is slower (Fig. ~~2a3a,~~ negative slopes of solid and dashed lines), consistent with Fig. ~~1~~
249 ~~2~~ (e.g., steepening from dark blue to light blue curves in Figs. ~~1a2a,b~~). In particular, ~~it the gradient~~ approximately follows a
250 negative power law as a function of ramping rate on both warming and cooling time series (~~dashed and solid lines in Fig. 2a~~).
251 ~~In Scenario 3, the maximum gradient is nearly insensitive to the ramping rate (relatively flat dash-dotted lines).~~ In Fig. ~~2b3b,~~
252 we see a similar result for the simple ODE, as seen by the shallowing of the power law from Scenarios 1 to 3 (though here
253 the slope in Scenario 3 is clearly nonzero). Notably, ~~the in the cubic ODE the~~ power law in the case with the largest region
254 of bi-stability (Scenario 1) is approximately given by $\max(dx/d\beta) \propto \mu^{-1}$, where μ again is the ramping rate. The Supporting
255 Information further explains the above convergence rate of μ^{-1} .

256 A dependence of the maximum gradient on (ramping rate)⁻¹ in the case of wide bi-stability suggests that running a climate
257 model with twice as gradual CO₂ ramping ~~;~~ leads to less than a factor of two increase in the gradient $\max(dV/dCO_2)$. This
258 is an important result because this implies that the distance between the CO₂ at the simulated transient “tipping point” and the
259 CO₂ of the true (equilibrium) tipping point (which we want to estimate) also only reduces by a factor of two ~~;~~ when the ramping
260 rate is reduced by a factor of two. A greater power law slope (e.g., a slope of -2) would imply a much faster convergence to
261 the equilibrium location of the tipping point. Thus, using more and more gradual ramping experiments may be an inefficient
262 way to approach the equilibrium behavior of ~~a physical system. The Supplementary Information further explains the above~~
263 ~~convergence rate of μ^{-1} this physical system, suggesting the need for a more efficient approach, discussed next.~~

264 3.3 Predicting the steady-state behavior of sea ice using only transient runs

265 ~~One of our key results~~

266 Our main novel result, presented next, is a method for finding the CO₂ concentration at which a bifurcation (if any) occurs
267 in the equilibrium ~~and estimating the associated hysteresis width~~ using computationally feasible transient model runs instead
268 of fixed-forcing steady-state runs. We are interested in this CO₂ concentration because it determines the threshold beyond
269 which significant sea ice loss is practically irreversible ~~Ritchie et al. (2021). In~~ (Ritchie et al., 2021). In our simple, inexpensive
270 model, we can test the estimates of the bi-stability and associated tipping points derived from transient model runs against the
271 known true tipping points and equilibrium structure that are found from fixed-forcing runs (see Methods). When used in a
272 GCM, our method would provide a prediction for the existence and location of tipping points when the equilibrium value of
273 sea ice is actually unknown. Thus, this section is a proof of concept that our new method can accurately determine whether
274 observed rate-dependent hysteresis is caused by lag around a system with no bi-stability or tipping points or caused by a
275 rate-dependent widening of an equilibrium hysteresis loop in a system with tipping points.

276 In Fig. 3a4a, we plot a measure of the upper and lower CO₂ values ~~of the upper and lower that correspond to the rightmost~~
277 and leftmost edges of the ~~transient rate-dependent~~ hysteresis (by calculating the CO₂ at which the March sea ice area crosses a
278 critical threshold, see Methods and Supplementary Figure S9). We plot this threshold for the warming (increasing greenhouse
279 concentration) trajectories in blue (CO₂ⁱ) and for the cooling (decreasing greenhouse) trajectories in red (CO₂^d), as a function
280 of the ramping rate for all three scenarios. As expected, as the ramping rate gets slower CO₂ⁱ and CO₂^d asymptote to the CO₂
281 values corresponding to the edges of ~~bi-stability the equilibrium hysteresis~~ and the location of the true tipping points in the
282 case of Scenarios 1 and 2 (denoted by the × symbols). In Scenario 3, CO₂ⁱ and CO₂^d asymptote to the same value (~~transient the~~
283 rate-dependent hysteresis width approaches zero) because there is no bi-stability in the steady-state.

284 Finally, we demonstrate that fitting a curve to the edges of the ~~transient rate-dependent~~ hysteresis (CO₂ⁱ and CO₂^d) as a
285 function of the ramping rate can be used to predict CO₂ⁱ and CO₂^d at infinitely slow ramping rates ~~;~~ and therefore (i.e., the edges
286 of the equilibrium hysteresis). This would allow us to estimate the CO₂ value corresponding to a bifurcation in the equilibrium
287 behavior without running a model to a ~~steady-state~~ steady state. In Fig. 3a-4a, we plot CO₂ⁱ and CO₂^d, and the curves that fit
288 them (see Methods) as functions of the ramping rate, and the predicted values of CO₂ⁱ and CO₂^d at infinitely slow ramping rates
289 with a 95% confidence interval range shaded around them. We perform this fitting and estimation process using all the ramping

290 experiments (18 different ramping rates total, as shown in Fig. 3a4a). We then repeat the fit using fewer and fewer experiments
291 to explore how the uncertainty on predicted values of CO_2^i and CO_2^d increases as we move to only using a few fast ramping
292 experiments that are more feasible when using full complexity climate models. Fig. 3b-4b shows a summary of these analyses.

293 The predicted values of CO_2^i and CO_2^d are remarkably accurate for all scenarios (points approaching the red and blue \times in
294 Fig. 3b4b), even when excluding several of the slower ramping experiments. This is an important test because when this method
295 is applied to a GCM, one would only have a smaller number of faster ramping experiments due to computational limitations.
296 The uncertainties (indicated by the shaded blue and red bars around the points) in the predictions grow when excluding more
297 experiments from the curve fitting process but still remain very low, especially for Scenarios 1 and 2. In predicting CO_2^d for
298 Scenario 3, the uncertainties are a bit higher because the exponential-functional form of our fit does not represent this case
299 as well as the others, leading to serial correlation in the residuals. The structure in the residuals can be used to guide the
300 choice of the functional form used to fit such data in future applications. This same method and functional form can also
301 successfully predict the equilibrium structure of our simple ODE (Eqn. 1), with even smaller uncertainties on the prediction
302 when using very few ramping experiments (see Figure S11). Finally, we can use the difference of the distributions CO_2^i
303 and CO_2^d to calculate the probability that bi-stability—and bi-stability—and thus a tipping point—exists (see Supplementary
304 point—exists (see Supporting Information). Another very similar approach using only the difference between CO_2^i and CO_2^d
305 (i.e., the hysteresis width) as a function of the ramping rate is also shown in Figure S10.

306 Overall, these results demonstrate the potential for using several shorter runs with time-changing CO_2 forcing to efficiently
307 estimate the CO_2 value of the tipping points and predict the existence of bi-stability in GCMs where equilibrium runs or long,
308 slow-ramping hysteresis runs are computationally infeasible.

309 4 Discussion

310 We have shown that it is not feasible to use a single climate model hysteresis run with time-changing (transient) forcing to
311 cannot be used to conclusively estimate the true location of Arctic winter sea ice tipping points, the range of bi-stability in the
312 steady-state, and even the existence of bi-stability at all, consistent with the findings of Li et al. (2013). We also showed that this
313 seems to be a general issue in nonlinear systems, as the same problem occurs in a generic ODE undergoing transient hysteresis.
314 Examining the maximum gradient of sea ice thickness with respect to, We demonstrated that the transient sea-ice responses
315 under a time-changing CO_2 as a function of the ramping rate of CO_2 , we reflect the generic behavior of a nonlinear dynamical
316 system (e.g., our Eqn. 1): specifically, we showed that systems with and without bi-stability can also produce qualitatively
317 indistinguishable rate-dependent hysteresis behavior. We also find that very long model runs are needed to identify whether this
318 value approaches infinity, which would indicate a bifurcation, the system approaches a bifurcation (Fig. 3) and at what CO_2 this
319 occurs. We showed that even in runs with a very slow-changing CO_2 , the system can be surprisingly far from the equilibrium as
320 it undergoes a tipping point, consistent with the work of Li et al. (2013). In addition, even with a very slow ramping experiment,
321 one would always have to perform additional expensive fixed-forcing experiments (as done by Li et al., 2013) to confirm that
322 the experiment was indeed in quasi-equilibrium. Instead, we propose using a a novel method that uses a few fast-ramping

323 experiments to efficiently predict the true range of bi-stability and provide uncertainty estimates on this prediction. ~~The ramping~~
324 ~~rates used here likely represent an upper bound for applying our method to GCMs (for example,~~

325 We demonstrated that the method we propose can accurately predict the steady-state behavior of sea ice in a simple model;
326 now we discuss applying this method to a GCM. First, we note that while we use a highly idealized model of sea ice in this
327 study, the method developed deals with identifying bi-stability in complex systems with unknown equilibrium structures more
328 generally. This means that the framework should be applicable to other models (including GCMs), since moving from fast to
329 slower ramping rates allows convergence to the equilibrium behavior. It could also be used in the context of the abrupt transition
330 vastly different climate problems, for example, in identifying the abrupt transitions to a moist greenhouse (Popp et al., 2016),
331 runaway greenhouse (Goldblatt et al., 2013), or snowball Earth state (Hyde et al., 2000));~~as we expect GCMs to have longer~~
332 ~~equilibration timescales than the idealized Eisenman sea ice model.~~

333 ~~We demonstrated that the method we propose can accurately predict the steady-state behavior of sea ice in a simple model;~~
334 ~~however, several challenges remain to deploying this method for use in full-complexity models. GCMs contain.~~ The functional
335 form used to fit the transient runs, as well as the level of certainty achieved from a given number of experiments, would likely
336 depend on the given model and climate problem analyzed. Possible challenges in finding the functional best fit to the transient
337 runs might mirror those of Gregory et al. (2004) who encountered difficulties when trying to fit a line to un-equilibrated GCM
338 runs with a different goal of deducing the equilibrium climate sensitivity. We suggest that a careful examination of the residuals
339 from a given fit can help guide the choice of functional form.

340 The generality of the method also highlights another advantage: the same set of ramping experiments in a GCM could be
341 used to analyze all suspected tipping elements in the Earth's climate system simultaneously. The main challenge we anticipate
342 in applying this method to GCMs comes from the significant stochastic variability and multiple timescales of forcings that
343 may render the calculated values of the diagnostics used here (such as the width of the transient hysteresis) uncertain. ~~In~~
344 ~~addition, the functional form to fit to CO_2^i and CO_2^d rate-dependent hysteresis more uncertain in a GCM may require some~~
345 ~~further experimenting (such as trying an exponential rather than polynomial form) due to the more complex sea ice dynamics~~
346 ~~of the GCM. Nonetheless, we argue that~~ using multiple runs to estimate the width of the bi-stability of a given climate variable
347 and ~~provide~~ providing a quantified uncertainty on such a prediction ~~offers~~ should offer a potential improvement over using a
348 single hysteresis experiment. ~~This approach still requires significant computational resources due to the need to run the model~~
349 ~~to equilibrium after the ramping up and ramping down of~~

350 We can estimate the efficiency of the proposed approach over more standard ones when applied in a GCM. Taking the
351 experimental setup of Li et al. (2013) as a guide, we can assume that a slow-ramping experiment to $4 \times \text{CO}_2$ requires a 2000-year
352 ramp up and ramp down with at minimum a 2500-year equilibration period after each ramp (though they actually allowed the
353 model to equilibrate for nearly 6000 years). Within the 500 ppm width of the rate-dependent hysteresis found by Li et al. (2013)
354 , ten fixed-forcing experiments 2500 years long would be needed to test for bi-stability and estimate the tipping point location
355 at a relatively crude accuracy of 100 ppm. This leads to a total of 34,000 simulation years. On the other hand, if we used
356 our proposed approach, we could run three ramping experiments with fast to intermediate rates of 100, 200, and 400 years to
357 quadruple CO_2 in a hysteresis experiment. We would run only one experiment to complete equilibration after ramp up (2500

358 years) and run the others only until they lost their sea ice, using the ice-free steady-state run to conduct the three ramp downs.
359 This yields a total of approximately 6400 simulation years and computational savings by over a factor of 5. Using only three
360 ramping experiments is sufficient to get an estimate of the equilibrium hysteresis width and location, but the uncertainty of the
361 estimate could still be high.

362 ~~Previous work~~ Finally, our results indicate that rate-dependent hysteresis and irreversibility of Arctic winter sea ice are
363 expected to be relevant for realistic rates of CO₂ increase. While rate-dependent hysteresis has been explored in other climate
364 contexts (e.g., AMOC, Kim et al., 2021; An et al., 2021), previous work on Arctic winter sea ice has typically sought to iden-
365 tify ~~bi-stability equilibrium hysteresis~~ in sea ice because it would imply irreversibility of sea ice loss ~~(in the sense that CO₂~~
366 ~~would have to be reduced beyond the tipping point value to allow sea ice re-growth).~~ Here, we highlight a different perspective
367 ~~by focusing on realistic rates of CO₂ increase in addition to the steady-state, generally ignoring the out-of-equilibrium~~ behav-
368 ior of sea ice under rapid CO₂ changes. The SSP585 Scenario in CMIP6 corresponds to a ramping rate of approximately 60
369 years per CO₂ doubling: a rate at which sea ice in our idealized model already exhibits rate-dependent hysteresis, that is, sig-
370 nificant deviation from its steady state (60 years per doubling would fall between the 25 see Figs. 2 and 100 years per doubling
371 blue curves in Figure 1, see also Fig. S2). Since we identify transient rate-dependent hysteresis in sea ice here in all scenar-
372 ios, even without a deep ocean and subsequent recalcitrant warming (Held et al., 2010), we expect ~~transient rate-dependent~~
373 hysteresis to be even more pronounced in GCMs and in the real climate when such long-timescale components are included.
374 ~~We therefore conclude that irreversibility, therefore, conclude that on policy-relevant timescales~~ the significant irreversibility
375 of winter Arctic sea ice involved in rate-dependent hysteresis is likely to occur in the real climate system due to the expected
376 lagged response regardless of whether an actual bifurcation (tipping point) in the equilibrium exists.

377 *Code availability.* An implementation of the Eisenman 2007 sea ice model in python used for this study can be found on Zenodo at:
378 <https://doi.org/10.5281/zenodo.6708812> (Hankel, 2022).

379 *Author contributions.* CH and ET designed the research project and prepared the manuscript together, CH implemented the model and
380 conducted the experiments.

381 *Competing interests.* The authors declare no competing interests.

382 *Acknowledgements.* The authors would like to thank Ian Eisenman for his helpful input during the project and for the guidance in using
383 his sea ice model. We thank the anonymous reviewers for their constructive feedback. ET thanks the Weizmann Institute for its hospitality
384 during parts of this work. This work has been funded by the NSF Climate Dynamics program (joint NSF/NERC) grant AGS-1924538.

385 **References**

- 386 Abbot, D. S. and Tziperman, E.: Sea ice, high-latitude convection, and equable climates, *Geophysical Research Letters*, 35, 2008.
- 387 Abbot, D. S., Walker, C., and Tziperman, E.: Can a convective cloud feedback help to eliminate winter sea ice at high CO₂ concentrations?,
388 *J. Climate*, 22, 5719–5731, <https://doi.org/10.1175/2009JCLI2854.1>, 2009.
- 389 An, S.-I., Kim, H.-J., and Kim, S.-K.: Rate-Dependent Hysteresis of the Atlantic Meridional Overturning Circulation System and Its Asym-
390 metric Loop, *Geophysical Research Letters*, 48, e2020GL090132, 2021.
- 391 Armour, K., Eisenman, I., Blanchard-Wrigglesworth, E., McCusker, K., and Bitz, C.: The reversibility of sea ice loss in a state-of-the-art
392 climate model, *Geophysical Research Letters*, 38, 2011.
- 393 Baer, S. M., Erneux, T., and Rinzel, J.: The slow passage through a Hopf bifurcation: delay, memory effects, and resonance, *SIAM Journal*
394 *on Applied mathematics*, 49, 55–71, 1989.
- 395 Bathiany, S., Notz, D., Mauritsen, T., Raedel, G., and Brovkin, V.: On the potential for abrupt Arctic winter sea ice loss, *Journal of Climate*,
396 29, 2703–2719, 2016.
- 397 Bathiany, S., Scheffer, M., Van Nes, E., Williamson, M., and Lenton, T.: Abrupt climate change in an oscillating world, *Scientific reports*, 8,
398 1–12, 2018.
- 399 Boers, N.: Observation-based early-warning signals for a collapse of the Atlantic Meridional Overturning Circulation, *Nature Climate*
400 *Change*, 11, 680–688, 2021.
- 401 Breban, R., Nusse, H. E., and Ott, E.: Lack of predictability in dynamical systems with drift: scaling of indeterminate saddle-node bifurca-
402 tions, *Physics Letters A*, 319, 79–84, 2003.
- 403 Burt, M. A., Randall, D. A., and Branson, M. D.: Dark warming, *Journal of Climate*, 29, 705–719, 2016.
- 404 Comiso, J. C. and Parkinson, C. L.: Satellite observed changes in the Arctic, *Physics Today*, 2004.
- 405 Curry, J. A., Schramm, J. L., and Ebert, E. E.: Sea ice–albedo climate feedback mechanism, *J. Climate*, 8, 240–247, 1995.
- 406 Ditlevsen, P. D. and Johnsen, S. J.: Tipping points: Early warning and wishful thinking, *Geophys. Res. Lett.*, 37, 2010.
- 407 Eisenman, I.: Arctic catastrophes in an idealized sea ice model, 2006 Program of Studies: Ice (Geophysical Fluid Dynamics Program), pp.
408 133–161, 2007.
- 409 Eisenman, I.: Factors controlling the bifurcation structure of sea ice retreat, *Journal of Geophysical Research: Atmospheres*, 117, 2012.
- 410 Eisenman, I. and Wettlaufer, J. S.: Nonlinear threshold behavior during the loss of Arctic sea ice, *Proc Nat Acad Sci USA*, 106, 28–32, 2009.
- 411 Feldl, N., Po-Chedley, S., Singh, H. K., Hay, S., and Kushner, P. J.: Sea ice and atmospheric circulation shape the high-latitude lapse rate
412 feedback, *npj Climate and Atmospheric Science*, 3, 1–9, 2020.
- 413 Ghil, M. and Childress, S.: *Topics in Geophysical Fluid Dynamics: Atmospheric Dynamics, Dynamo Theory and Climate Dynamics*,
414 Springer-Verlag, New York, 1987.
- 415 Goldblatt, C., Robinson, T. D., Zahnle, K. J., and Crisp, D.: Low simulated radiation limit for runaway greenhouse climates, *Nature Geo-*
416 *science*, 6, 661–667, 2013.
- 417 Gregory, J., Ingram, W., Palmer, M., Jones, G., Stott, P., Thorpe, R., Lowe, J., Johns, T., and Williams, K.: A new method for diagnosing
418 radiative forcing and climate sensitivity, *Geophysical research letters*, 31, 2004.
- 419 Haberman, R.: Slowly varying jump and transition phenomena associated with algebraic bifurcation problems, *SIAM Journal on Applied*
420 *Mathematics*, 37, 69–106, 1979.
- 421 Hankel, C.: *camillehankel/sea_ice_thermo_0d: 0D-Sea-Ice-Model*, <https://doi.org/10.5281/zenodo.6708812>, 2022.

422 Hankel, C. and Tziperman, E.: The Role of Atmospheric Feedbacks in Abrupt Winter Arctic Sea Ice Loss in Future Warming Scenarios,
423 *Journal of Climate*, 34, 4435–4447, 2021.

424 Hartmann, D. L.: *Global physical climatology*, vol. 103, chap. Chapter 2, Newnes, 2015.

425 Held, I. M., Winton, M., Takahashi, K., Delworth, T., Zeng, F., and Vallis, G. K.: Probing the fast and slow components of global warming
426 by returning abruptly to preindustrial forcing, *Journal of Climate*, 23, 2418–2427, 2010.

427 Hezel, P., Fichefet, T., and Massonnet, F.: Modeled Arctic sea ice evolution through 2300 in CMIP5 extended RCPs, *The Cryosphere*, 8,
428 1195–1204, 2014.

429 Holland, M. M., Bitz, C. M., and Tremblay, B.: Future abrupt reductions in the summer Arctic sea ice, *Geophysical Research Letters*, 33,
430 2006.

431 Hyde, W. T., Crowley, T. J., Baum, S. K., and Peltier, W. R.: Neoproterozoic ‘snowball Earth’ simulations with a coupled climate/ice-sheet
432 model, *Nature*, 405, 425–429, 2000.

433 Kaszás, B., Feudel, U., and Tél, T.: Tipping phenomena in typical dynamical systems subjected to parameter drift, *Scientific reports*, 9, 8654,
434 2019.

435 Kay, J. E., Holland, M. M., Bitz, C. M., Blanchard-Wrigglesworth, E., Gettelman, A., Conley, A., and Bailey, D.: The influence of local
436 feedbacks and northward heat transport on the equilibrium Arctic climate response to increased greenhouse gas forcing, *Journal of Climate*,
437 25, 5433–5450, 2012.

438 Kim, H.-J., An, S.-I., Kim, S.-K., and Park, J.-H.: Feedback processes modulating the sensitivity of Atlantic thermohaline circulation to
439 freshwater forcing timescales, *Journal of Climate*, 34, 5081–5092, 2021.

440 Kwok, R. and Untersteiner, N.: The thinning of Arctic sea ice, *Phys. Today*, 64, 36–41, 2011.

441 Lavergne, T., Sørensen, A. M., Kern, S., Tonboe, R., Notz, D., Aaboe, S., Bell, L., Dybkjær, G., Eastwood, S., Gabarro, C., et al.: Version 2
442 of the EUMETSAT OSI SAF and ESA CCI sea-ice concentration climate data records, *The Cryosphere*, 13, 49–78, 2019.

443 Leibowicz, B. D., Abbot, D. S., Emanuel, K. A., and Tziperman, E.: Correlation between present-day model simulation of Arc-
444 tic cloud radiative forcing and sea ice consistent with positive winter convective cloud feedback, *J. Adv. Model. Earth Syst.*, 4,
445 <https://doi.org/10.1029/2012MS000153>, 2012.

446 Lenton, T. M.: Arctic climate tipping points, *Ambio*, 41, 10–22, 2012.

447 Li, C., Notz, D., Tietsche, S., and Marotzke, J.: The transient versus the equilibrium response of sea ice to global warming, *Journal of Climate*,
448 26, 5624–5636, 2013.

449 Lindsay, R. and Schweiger, A.: Arctic sea ice thickness loss determined using subsurface, aircraft, and satellite observations, *The Cryosphere*,
450 9, 269–283, 2015.

451 Mandel, P. and Erneux, T.: The slow passage through a steady bifurcation: delay and memory effects, *Journal of statistical physics*, 48,
452 1059–1070, 1987.

453 Manoli, G., Faticchi, S., Bou-Zeid, E., and Katul, G. G.: Seasonal hysteresis of surface urban heat islands, *Proceedings of the National
454 Academy of Sciences*, 117, 7082–7089, 2020.

455 Nghiem, S., Rigor, I., Perovich, D., Clemente-Colón, P., Weatherly, J., and Neumann, G.: Rapid reduction of Arctic perennial sea ice,
456 *Geophysical Research Letters*, 34, 2007.

457 Notz, D.: The future of ice sheets and sea ice: Between reversible retreat and unstoppable loss, *Proceedings of the National Academy of
458 Sciences*, 106, 20590–20595, 2009.

459 Notz, D. and Stroeve, J.: Observed Arctic sea-ice loss directly follows anthropogenic CO₂ emission, *Science*, 354, 747–750, 2016.

460 Park, D.-S. R., Lee, S., and Feldstein, S. B.: Attribution of the recent winter sea ice decline over the Atlantic sector of the Arctic Ocean,
461 *Journal of Climate*, 28, 4027–4033, 2015.

462 Popp, M., Schmidt, H., and Marotzke, J.: Transition to a moist greenhouse with CO₂ and solar forcing, *Nature communications*, 7, 1–10,
463 2016.

464 Ridley, J., Lowe, J., and Hewitt, H.: How reversible is sea ice loss?, *The Cryosphere*, 6, 193, 2012.

465 Ritchie, P. D., Clarke, J. J., Cox, P. M., and Huntingford, C.: Overshooting tipping point thresholds in a changing climate, *Nature*, 592,
466 517–523, 2021.

467 Stroeve, J. and Notz, D.: Changing state of Arctic sea ice across all seasons, *Environmental Research Letters*, 13, 103 001, 2018.

468 Stroeve, J., Serreze, M., Drobot, S., Gearheard, S., Holland, M., Maslanik, J., Meier, W., and Scambos, T.: Arctic sea ice extent plummets in
469 2007, *Eos, Transactions American Geophysical Union*, 89, 13–14, 2008.

470 Stroeve, J. C., Serreze, M. C., Holland, M. M., Kay, J. E., Malanik, J., and Barrett, A. P.: The Arctic’s rapidly shrinking sea ice cover: a
471 research synthesis, *Climatic change*, 110, 1005–1027, 2012.

472 Strogatz, S.: *Nonlinear dynamics and chaos*, Westview Press, 1994.

473 Tredicce, J. R., Lippi, G. L., Mandel, P., Charasse, B., Chevalier, A., and Picqué, B.: Critical slowing down at a bifurcation, *American Journal*
474 *of Physics*, 72, 799–809, 2004.

475 Wagner, T. J. and Eisenman, I.: How climate model complexity influences sea ice stability, *Journal of Climate*, 28, 3998–4014, 2015.

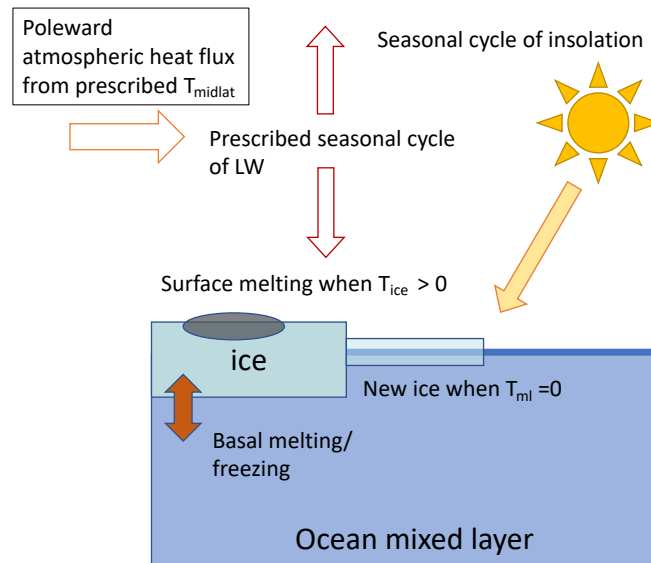


Figure 1. Transient hysteresis runs (time-changing forcing) and equilibrium runs (fixed forcing) for average March sea ice effective thickness (sea ice volume divided by area. Schematic showing some of the grid cell; panels a,e,d) and the simple ODE from Eq. 1 (b,d,f). The first row corresponds to Scenario 1 (wide bi-stability), the second row to Scenario 2 (narrow bi-stability), and the third to Scenario 3 (no bi-stability). Blue lines indicate simulations with increasing forcing (CO_2 or β), while red lines indicate simulations with decreasing forcing. Dashed and dotted black lines indicate the steady-state values key features of sea ice or the ODE variable x Eisenman (2007) model. These two black lines Its four prognostic variables are different when the two initial conditions evolve to two different steady-states. The legends indicate the different ramping rates (represented by darker colors for faster rates): ice volume, which are in units of years per CO_2 doubling in the case of the sea ice model. The green arrows demonstrate the direction of evolving sea area, ice effective thickness during the transient hysteresis experiments surface temperature, and ocean mixed layer temperature.

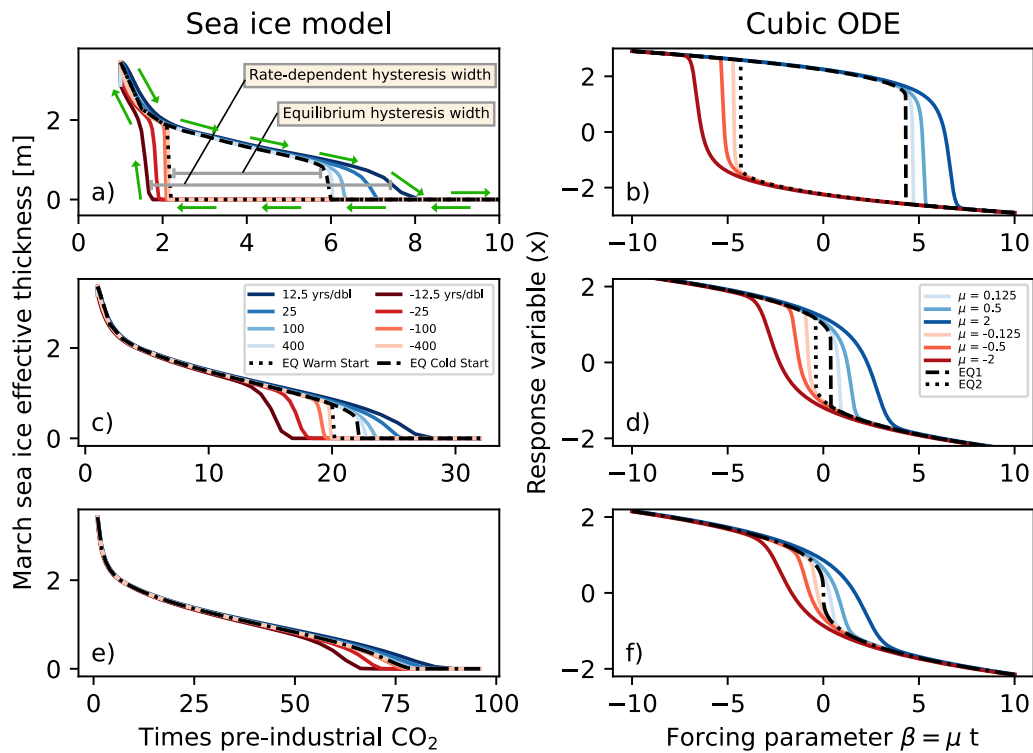


Figure 2. Hysteresis runs (time-changing forcing) and equilibrium runs (fixed forcing) for average March sea ice effective thickness (sea ice volume divided by area of the grid cell; panels a,c,d) and the simple ODE from Eq. 1 (b,d,f). The first row corresponds to Scenario 1 (wide bi-stability), the second row to Scenario 2 (narrow bi-stability), and the third to Scenario 3 (no bi-stability). Blue lines indicate simulations with increasing forcing (CO₂ or β), while red lines indicate simulations with decreasing forcing. Dashed and dotted black lines indicate the steady-state values of sea ice or the ODE variable x . These two black lines are different when the two initial conditions evolve to two different steady-states. The legends indicate the different ramping rates (represented by darker colors for faster rates), which are in units of years per CO₂ doubling in the case of the sea ice model. The green arrows demonstrate the direction of evolving sea ice effective thickness during the hysteresis experiments.

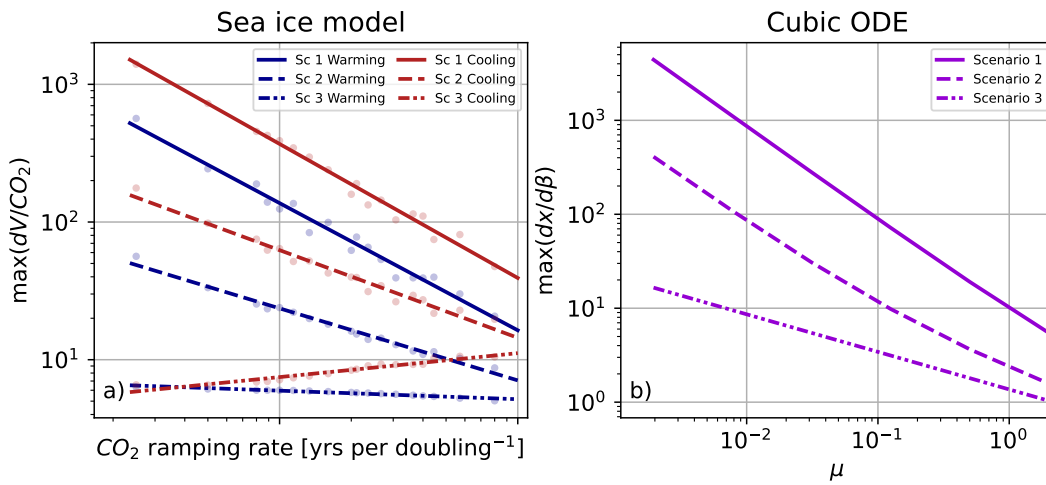


Figure 3. Maximum gradient of sea ice effective thickness with respect to CO_2 in panel a, and the maximum gradient of x with respect to the forcing parameter β in panel b during transient simulations. For the sea ice model (a) the data points from the 18 different runs are shown as faded points, with a superimposed line of best fit. For the cubic ODE (b) the maximum gradient lines corresponding to increasing and decreasing forcing time series are identical due to the symmetry around $\beta = 0$ seen in Fig. 1b, d, and f.

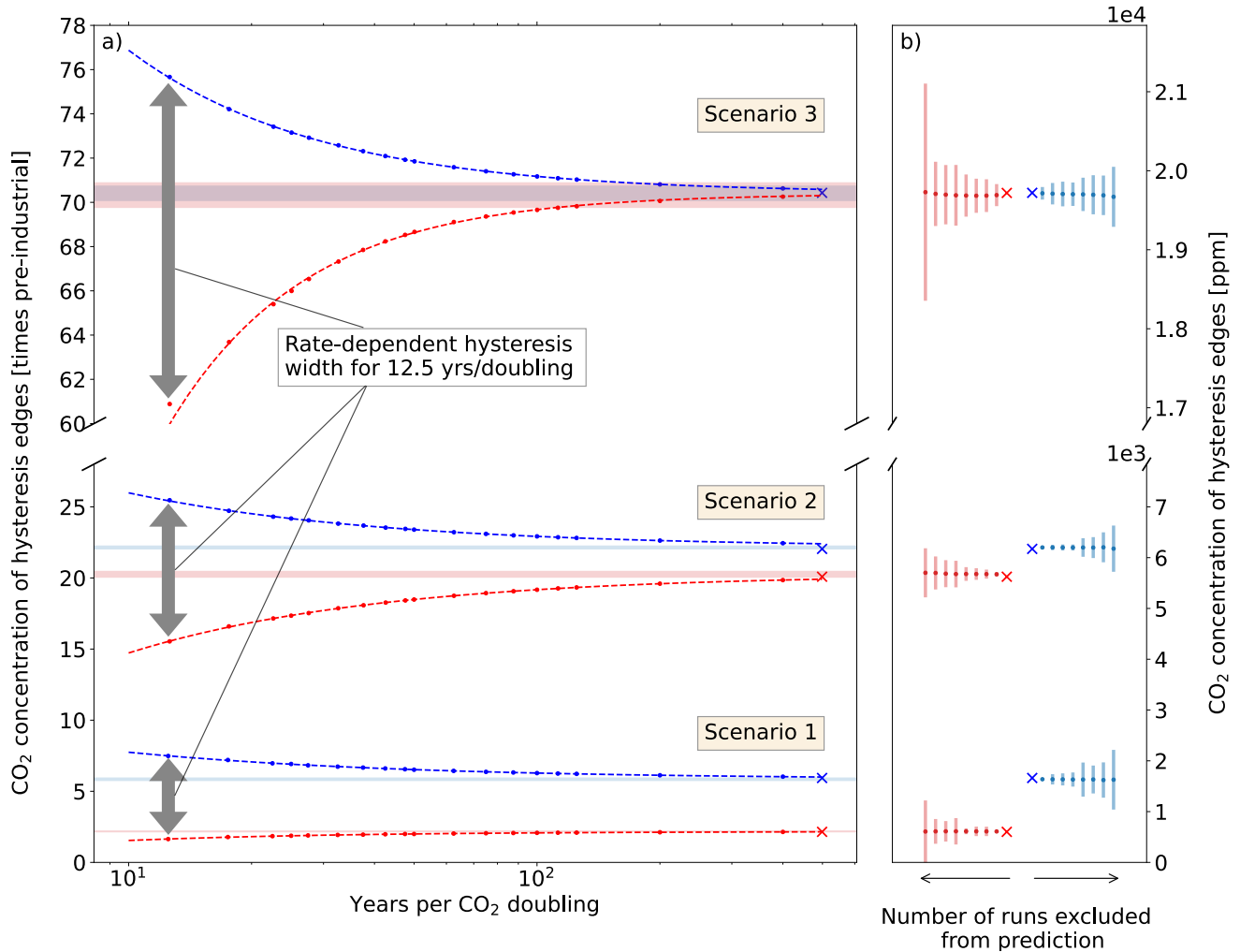


Figure 4. Estimating the equilibrium tipping point value from the transient rate-dependent hysteresis runs. In panel a, the scatter points show the CO₂ value of the right and left edges of the transient rate-dependent hysteresis (CO₂ⁱ and CO₂^d, located along increasing (blue) and decreasing (red) CO₂ time-series respectively) for different ramping rates. The dashed lines show the curve that is fitted to the scatter points, and the shaded blue and red bands show $\pm 2\sigma$ around the predicted values of CO₂ⁱ and CO₂^d at infinitely slow ramping rates. The blue and red 'x's show the true equilibrium values of CO₂ⁱ and CO₂^d (calculated from the fixed CO₂ runs starting with cold and warm initial conditions respectively). In panel b, we analyze the accuracy of this prediction as we use fewer transient runs. For the three scenarios, we show the result of sequentially excluding the most gradual ramping simulations from the curve-fitting process used for predictions. The dots and the corresponding bars represent the predicted equilibrium values of CO₂ⁱ and CO₂^d, and $\pm 2\sigma$ around the prediction, and dots moving away from the true value with larger error bars correspond to excluding more and more runs from the calculation.